

Revealing the anisotropic charge-density-wave order of TiSe_2 through high harmonic generation

Lin Zhang,¹ Igor Tyulnev,¹ Lenard Vamos,¹ Julita Poborska,¹ Utso Bhattacharya,²
Ravindra W. Chhajlany,³ Tobias Grass,^{4,5} Jens Biegert,^{1,6} and Maciej Lewenstein^{1,6}

¹*ICFO-Institut de Ciències Fòniques, The Barcelona Institute of Science and Technology,
Av. Carl Friedrich Gauss 3, 08860 Castelldefels (Barcelona), Spain*

²*Institute for Theoretical Physics, ETH Zurich, Zurich, Switzerland*

³*ISQI - Institute of Spintronics and Quantum Information,
Faculty of Physics and Astronomy, Adam Mickiewicz University, Poznań, Poland*

⁴*DIPC - Donostia International Physics Center,
Paseo Manuel de Lardizábal 4, San Sebastián, Spain*

⁵*Ikerbasque - Basque Foundation for Science, Maria Diaz de Haro 3, Bilbao, Spain*

⁶*ICREA, Pg. Lluís Companys 23, Barcelona, Spain*

Titanium diselenide (TiSe_2) is a transition-metal dichalcogenide material that undergoes a charge-density-wave (CDW) transition at $T_c \approx 200$ K. In a recent experiment [I. Tyulnev *et al.*, arXiv:2409.04216], the high harmonic generation (HHG) spectra of this material has been studied, which exhibits asymmetric behavior with respect to the polarization angle of the incident light and provides a new perspective to the CDW phase transition. In this work, we work out a theoretical explanation for the experimentally observed behavior of HHG spectra. We propose a simplified phenomenological mean-field model for this material, based on which the HHG spectra is calculated through the time-dependent Schrödinger equation. This model correctly describes the measured intensity distribution of the third-, fifth-, and seventh-order harmonic generation as a function of polarization direction and reveals a strong asymmetry due to the anisotropic CDW order in the low temperature phase. Our work provides a basis for applying high harmonic spectroscopy to reveal a new perspective on the nature of CDW orders.

Introduction.—High harmonic generation (HHG) is a nonlinear and nonperturbative optical process that occurs when intense laser fields interact with matter [1, 2]. This process leads to the ultrafast emission of high energy photons with frequencies being integer multiples of the initial driving frequency. HHG was initially discovered in the atomic and molecular gases and is the basis of attosecond science [3, 4]. The recent observation of HHG from solids has further renewed the interest in this field [5–14], which provides ultrafast time-resolved measurement about the driven material properties, such as the electron dynamics [15–18], the electron band properties [19–22], symmetries [23–27], and so on.

Theoretically, the HHG in solids is understood via the semiclassical single-active-electron three-step model [1, 2] adapted from the atomic HHG by assuming weak correlations or an effective single-particle picture, in which the electrons traverse the valence and conduction bands, creating and recombining with holes, producing a harmonic spectrum [14, 28–32]. Replacing these fundamental electrons with the many-body excitations such as the doublons and holons, the HHG can also be applied to study the properties of strongly correlated systems, such as the Mott insulator [33–37], Kitaev spin liquid [38], and high-temperature superconductor [39], in which the HHG spectra could be sensitive to the underlying different many-body phases and provides an all-optical probe of the quantum phase transitions [39, 40].

As a quasi-two-dimensional transition-metal

dichalcogenide material, the titanium diselenide (TiSe_2) undergoes a transition from the high temperature semimetal or semiconductor phase into a commensurate $2 \times 2 \times 2$ charge-density-wave (CDW) state at transition temperature $T_c \approx 200$ K [41]. Moreover, this material exhibits superconductivity with melting of the CDW upon the copper intercalation [42, 43], applying pressures [44, 45], or carrier doping [46, 47]. There is ongoing debate over the underlying mechanism, i.e., whether the CDW instability is driven by the electron-phonon coupling (Jahn-Teller effect) or exciton condensation [48–51]. Therefore, clarifying the properties of CDW order is significant for understanding this material. The very recent experiment of Ref. [52] shows that the HHG is highly sensitive to the CDW order and exhibits pronounced asymmetric behavior with respect to the polarization angle of the incident light. This provides a new perspective for studying the CDW phase transition.

In this Letter, we provide a theoretical explanation for the experimentally observed behavior of HHG spectra. Specifically, a simplified phenomenological mean-field model is proposed for the CDW phase, based on which the HHG spectra as a function of laser polarization angle are calculated. Our model correctly describes the measured behavior of harmonic orders as a function of the driving field polarization angle. The polarimetry sensitively detects the crystal orientation and explains the single-peaked behavior of the third-order (H3) and seventh-order (H7) harmonic generation as well as

the double-peaked behavior of the fifth-order harmonic generation (H5). Based on the excellent match between the experiment and theory, we reveal a strong asymmetry due to the anisotropic CDW order in the low temperature phase of the material. Our work theoretically explains the asymmetric behavior of HHG spectra observed in Ref. [52] and unveils that the HHG is sensitive to the CDW order.

Mean-field model.—We consider a simplified phenomenological mean-field model to describe the CDW order of TiSe₂. Like the exciton condensate model [53, 54], we consider only the highest lying valence band and the lowest lying conduction band within the minimal model for simplicity. The total Hamiltonian is expressed as

$$H = \sum_{\mathbf{k}} [\varepsilon_v(\mathbf{k}) - \mu] a_{\mathbf{k}}^\dagger a_{\mathbf{k}} + \sum_{\mathbf{k}} [\varepsilon_c(\mathbf{k}) - \mu] b_{\mathbf{k}}^\dagger b_{\mathbf{k}} + \sum_{\mathbf{Q}, \mathbf{k}} [\Delta_{(-\mathbf{Q})} a_{\mathbf{k}+\mathbf{Q}}^\dagger b_{\mathbf{k}} + \Delta_{(+\mathbf{Q})} b_{\mathbf{k}-\mathbf{Q}}^\dagger a_{\mathbf{k}}]. \quad (1)$$

Here $a_{\mathbf{k}}$ and $b_{\mathbf{k}}$ are the annihilation operator for the valence band and conduction band, respectively. The dispersions of valence band $\varepsilon_v(\mathbf{k})$ and conduction band $\varepsilon_c(\mathbf{k})$ are obtained from the tight-binding model introduced in Ref. [55] (see also End Matters for more details). As shown in Figs. 1(b) and 1(c), the valence band composed mainly of Se 4*p* orbitals gives rise to a hole pocket centered as Γ point, while the conduction band dominated by Ti 3*d* orbitals has three electron pockets centered at the M points. These pockets exhibit a small band overlap [see Fig. 1(d)], rendering a semimetal phase in the high-temperature regime of TiSe₂.

Below the critical temperature $T_c = 200$ K, the electron-electron and electron-phonon interactions further lead to a triple- \mathbf{Q} CDW order with wave vectors $|\mathbf{Q}_1| = |\mathbf{Q}_2| = |\mathbf{Q}_3| = \Gamma\text{M}$, which couple the hole pocket of valence band to the electron pockets of conduction band; see Fig. 1(c). In our phenomenological mean-field model (1), we model the CDW of TiSe₂ with the mean-field order parameters $\Delta_{(+\mathbf{Q})}$ while ignore the corresponding microscopic mechanism when studying the HHG spectra of this material. We assume that the CDW order parameter follows the mean-field temperature dependence considered in Ref. [56]:

$$\Delta(T) = \Delta_0 \sqrt{1 - (T/T_c)^2} \quad (2)$$

with $\Delta_0 = 115$ meV. The CDW order parameters fold the Brillouin zone; see Fig. 1(c). In the reduced Brillouin zone (RBZ), the mean-field Hamiltonian can be rewritten as

$$H = \sum_{\mathbf{k} \in \text{RBZ}} \Psi_{\mathbf{k}}^\dagger H(\mathbf{k}) \Psi_{\mathbf{k}}, \quad (3)$$

where $H(\mathbf{k})$ is the 8×8 momentum-dependent Hamiltonian matrix and we have the basis $\Psi_{\mathbf{k}} = (a_{\mathbf{k}}, b_{\mathbf{k}}, a_{\mathbf{k}+\mathbf{Q}_1}, b_{\mathbf{k}+\mathbf{Q}_1}, a_{\mathbf{k}+\mathbf{Q}_2}, b_{\mathbf{k}+\mathbf{Q}_2}, a_{\mathbf{k}+\mathbf{Q}_3}, b_{\mathbf{k}+\mathbf{Q}_3})^T$.

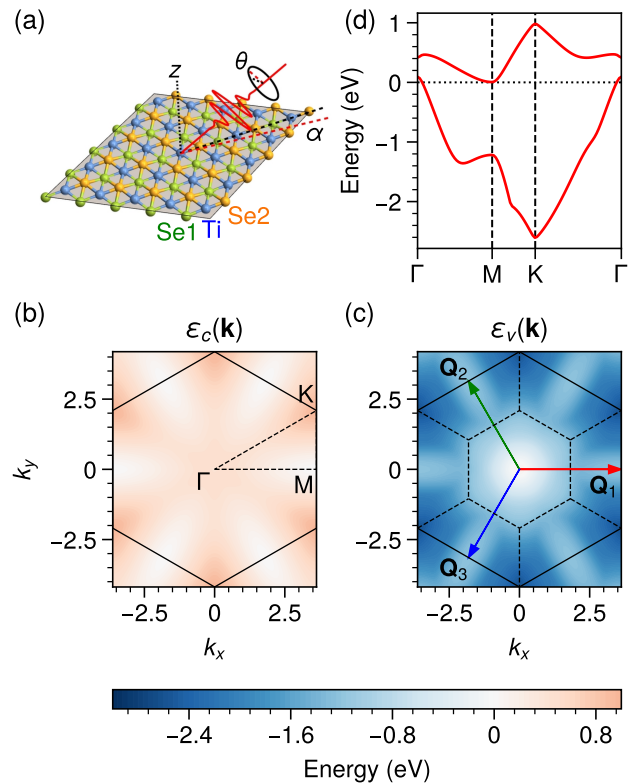


FIG. 1. Setup and tight-binding band structure of TiSe₂. (a) Laser geometric configuration. The laser pulse (solid red line) with linear polarization angle θ hits the material with an incident angle with respect to the material plane or the z axis, and the crystal axis (in-plane black dashed line) has an offset angle α compared to the in-plane incidence direction of the laser field (in-plane red dashed line). (b) (c) Contour plots of the lowest lying conduction band $\varepsilon_c(\mathbf{k})$ and the highest lying valence band $\varepsilon_v(\mathbf{k})$. The solid black hexagons represent the first Brillouin zone. In (c), we also show the wave vectors $\mathbf{Q}_{1,2,3}$ of the CDW order, which couple the hole pocket of valence band to the electron pockets of conduction band and fold the Brillouin zone. The dashed black lines represent the reduced Brillouin zone. (d) Band structure along the high-symmetry line [cf. (b)]. Here the Fermi energy E_F is set to zero.

HHG spectra.—To investigate the high harmonic spectra of the material, we couple the mean-field Hamiltonian $H(\mathbf{k})$ to an intense laser field described by the vector potential $\mathbf{A}(t)$ in dipole approximation through the minimal coupling scheme $\mathbf{k} \rightarrow \mathbf{k}(t) = \mathbf{k} + \mathbf{A}(t)$; see Fig. 1(a). Using the velocity gauge equation of motion in the Bloch basis [57], we have the following time-dependent Schrödinger equation for the density matrix $\rho(\mathbf{k}, t)$ at momentum \mathbf{k} :

$$\frac{d}{dt} \rho(\mathbf{k}, t) = -i[H(\mathbf{k} + \mathbf{A}(t); \{\Delta_{\mathbf{Q}_i}(t)\}), \rho(\mathbf{k}, t)]. \quad (4)$$

Here we explicitly express the dependence of the Bloch Hamiltonian on the time-evolved CDW order parameter

$\Delta_{\mathbf{Q}_i}(t) = (U_{\mathbf{Q}_i}/V) \sum_{\mathbf{k}} \text{Tr}[\rho(\mathbf{k}, t) a_{\mathbf{k}+\mathbf{Q}_i}^\dagger b_{\mathbf{k}}]$, with V the crystal volume and $U_{\mathbf{Q}_i}$ the effective interaction strength between electrons. The latter is taken as a phenomenological temperature-dependent parameter in our modeling to obtain suitable strength of the initial CDW order parameters self-consistently.

Initially, the system is in equilibrium, and the Fermi-Dirac distribution describes the occupation of each momentum mode, $\rho(\mathbf{k}, 0) = 1/[e^{H(\mathbf{k})/k_B T} + 1]$. Then, the system evolves according to the above equation of motion. We find it useful to introduce a phenomenological dephasing effect in the numerical simulation of HHG as follows [32]: After each time step δt of the evolution, we transform the density matrix into an adiabatic basis $U(\mathbf{k}, t)$ obtained by diagonalizing the instantaneous Hamiltonian $H(\mathbf{k} + \mathbf{A}(t); \{\Delta_{\mathbf{Q}_i}(t)\})$, i.e., $\tilde{\rho}(\mathbf{k}, t) = U^\dagger(\mathbf{k}, t)\rho(\mathbf{k}, t)U(\mathbf{k}, t)$. Then we apply the dephasing as $\tilde{\rho}_{mn}(\mathbf{k}, t) \rightarrow \tilde{\rho}_{mn}(\mathbf{k}, t)e^{-\delta t/\tau}$ for $m \neq n$ with τ being the dephasing time. Finally, we transform back to the Bloch basis.

With the time evolved density matrix $\rho(\mathbf{k}, t)$, we can calculate the expectation value of the velocity operator in direction j as

$$v_j(\mathbf{k}, t) = \text{Tr}[\rho(\mathbf{k}, t) \partial_{k_j} H(\mathbf{k} + \mathbf{A}(t); \{\Delta_{\mathbf{Q}_i}(t)\})]. \quad (5)$$

Denoting the direction of the laser field as \mathbf{n}_A and $v_j(t) = (1/V) \sum_{\mathbf{k}} v_j(\mathbf{k}, t)$, the high harmonic spectra can be obtained by the Fourier transform of the velocity (i.e., the current):

$$P(\omega) = \omega^2 |\text{FT}[\mathbf{v} \cdot \mathbf{n}_A]|^2. \quad (6)$$

In the following, we denote the spectrum strength at n th harmonic order as H_n .

We focus on the polarization dependence of the odd harmonic peaks (H3, H5, and H7). The results are organized along our main findings: (i) Unlike the spectra observed in Ref. [52], the harmonic spectra have a six-fold rotational symmetry for an incident laser field normal to the material plane. (ii) A better match with the experimental spectra is obtained when the laser field has an incident angle 45° with respect to the material plane, similar to the measurement geometry used in experiment. In particular, this choice reproduces a peak splitting characteristic of H5, which is absent in H3 and H7. (iii) The slight asymmetry between the H5 peaks in Ref. [52] is further reproduced when a small offset between the crystal axis and the p-polarization of the laser is introduced; see Fig. 1(a). (iv) To account for the much stronger H5 peak asymmetry experimentally observed in the low-temperature, we break the three-fold rotational symmetry of the mean-field CDW orders and find that tiny deviations from a symmetric mean field can result in a strongly asymmetric harmonic spectrum. In the following, we present the detailed results.

Normal incident field.—We first consider the incident laser field normal to the material plane, which is given by

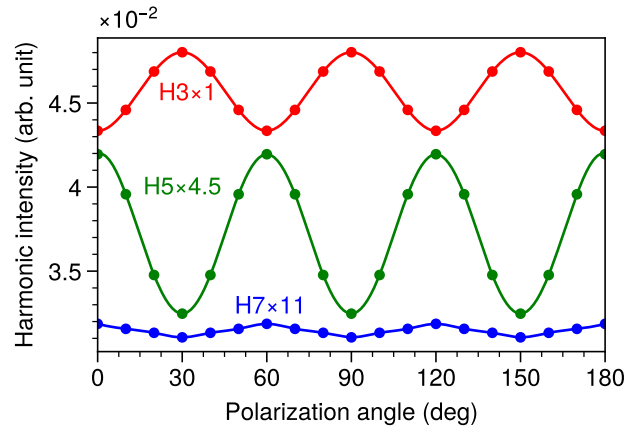


FIG. 2. HHG spectra as a function of polarization angle for the high temperature semimetal phase with the incident laser field normal to the material plane. Here we set $A_0 = 1.2$, $\omega = 0.4\text{eV}$, and $n_{\text{cyc}} = 8$.

the vector potential $\mathbf{A}(t) = A(t)[\cos(\theta - 60^\circ), \sin(\theta - 60^\circ)]$ with polarization angle θ . Here the p-polarized field with $\theta = 90^\circ$ is along the ΓK direction, and the field strength reads $A(t) = A_0 \sin^2(\frac{\omega t}{2n_{\text{cyc}}}) \sin(\omega t)$ with amplitude A_0 , center frequency ω , and cycle number n_{cyc} . We set $A_0 = 1.2$, $\omega = 0.4\text{eV}$, and $n_{\text{cyc}} = 8$ in this work. Fig. 2 shows the HHG spectra for the high temperature semimetal phase at $T = 300\text{K}$ with $\Delta_{\mathbf{Q}_i} = 0$. The HHG spectra is symmetric with respect to the polarization angle θ and shows three peaks in each harmonic order at 60° intervals, reflecting the hexagonal crystal symmetry of TiSe_2 . This behavior is different from the one observed in the experiment [52], where both H3 and H7 exhibit a single peak for the p-polarized laser field, while H5 splits into two symmetric peaks at 60° intervals. To understand the experimental behavior, we next consider the experimental laser geometric configuration with an incident angle 45° .

Laser field with incident angle 45° .—The vector potential for the laser field with incident angle 45° projected on the material plane reads $\mathbf{A}(t) = (A_x(t), A_y(t))$ with $A_x(t) = [\sin\theta \sin(60^\circ - \alpha) + (\sqrt{2}/2) \cos\theta \cos(60^\circ - \alpha)]A(t)$ and $A_y(t) = [\sin\theta \cos(60^\circ - \alpha) - (\sqrt{2}/2) \cos\theta \sin(60^\circ - \alpha)]A(t)$. Here the crystal axis offset α is also introduced in the laser field, describing the situation that the p-polarized field deviates from the ΓK direction; cf. Fig. 1(a). Compared with the normal incident field, the in-plane laser field amplitude now varies with the polarization angle θ , which is maximum when $\theta = 90^\circ$ and becomes minimized when $\theta = 0^\circ$. With this, the HHG spectra with three peaks shown in Fig. 2 should be deformed. Particularly, the HHG intensity away from the p-polarization $\theta = 90^\circ$ should be reduced.

In Fig. 3, we show the HHG spectra normalized by its maximal value for the high-temperature semimetal phase

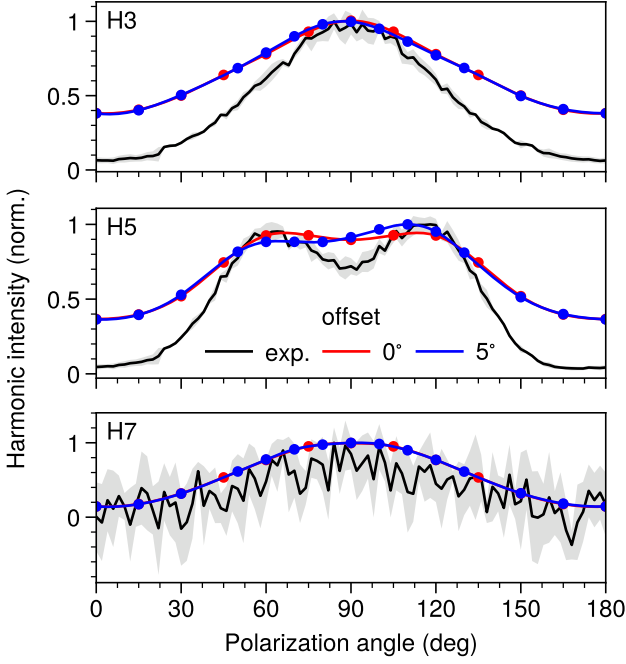


FIG. 3. Normalized HHG spectra of the high temperature semimetal phase for the laser field with incident angle 45° . Here the black lines represent the experimental data in Ref. [52] with the shaded area being the error bar. The red lines show the theoretical results without crystal axis offset, while the blue lines are obtained by introducing an offset $\alpha = 5^\circ$ in the numerical simulation. Here we set $A_0 = 1.2$, $\omega = 0.4$ eV, and $n_{\text{cyc}} = 8$.

with the laser incident angle 45° . The high harmonic H3 and H7 now exhibit a single peak around the polarization angle $\theta = 90^\circ$, while H5 splits into two symmetric peaks at $\theta = 30^\circ$ and $\theta = 120^\circ$ with interval 60° . This is close to the experimental results reported in Ref. [52]; cf. the black lines in Fig. 3. We note that in the experiment, a slight asymmetric behavior between the peaks in H5 is also observed. To explain this observation, we notice that the input laser field in the experiment has an offset angle $7^\circ \pm 2^\circ$ with respect to the crystal axis; cf. Fig. 1(a). After introducing an offset $\alpha = 5^\circ$ in our numerical simulation, the HHG spectra fits very well with the experimental results; see the blue curves in Fig. 3. Particularly, the left peak in H5 is lower than the right peak due to this offset. Therefore, the crystal axis offset could be responsible for the asymmetric behavior in the high-temperature phase.

We next consider the low-temperature CDW phase at 14 K. According to the mean-field CDW order parameter (2) considered in this work, we have the phenomenological effective interaction strength $U_{\mathbf{Q}_1} = U_{\mathbf{Q}_2} = U_{\mathbf{Q}_3} = -1.80935$ eV and the self-consistent CDW order parameter $\Delta_{\mathbf{Q}_1} = \Delta_{\mathbf{Q}_2} = \Delta_{\mathbf{Q}_3} = 0.1147$ eV. The corresponding HHG spectra normalized by the maximal value is shown in Fig. 4. Like the high temperature phase, H3 and H7 also have a single peak, while the

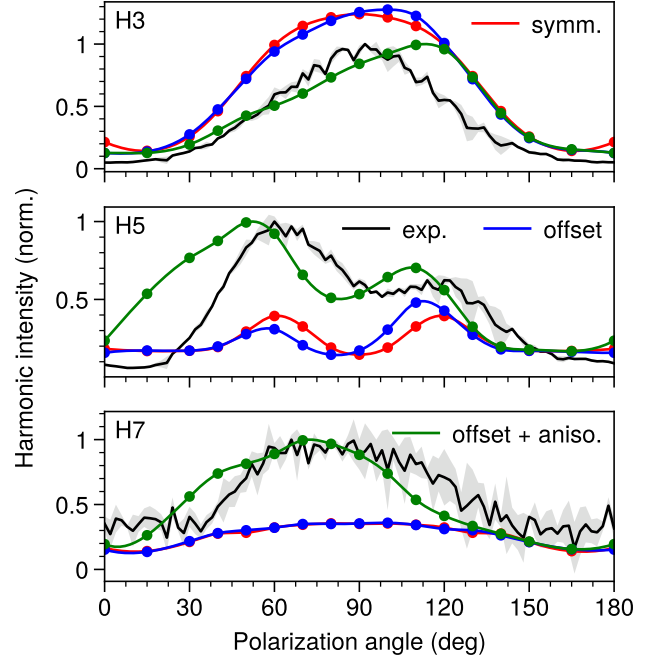


FIG. 4. Normalized HHG spectra of the low temperature CDW phase for the laser field with incident angle 45° . The black lines are the experimental results, while the colored lines are theoretical results. The red lines show the symmetric case with $\Delta_{\mathbf{Q}_1} = \Delta_{\mathbf{Q}_2} = \Delta_{\mathbf{Q}_3} = 0.1147$ eV, and the blue lines are obtained by introducing a crystal axis offset $\alpha = 5^\circ$. For the green lines, in addition to the offset $\alpha = 5^\circ$, we also introduced the anisotropic CDW order parameters $\Delta_{\mathbf{Q}_1} = 0.1148$ eV, $\Delta_{\mathbf{Q}_2} = 0.1147$ eV, and $\Delta_{\mathbf{Q}_3} = 0.1146$ eV. The parameters for the laser pulse are the same as in Fig. 3.

H5 splits into two symmetric peaks. Introducing an offset $\alpha = 5^\circ$ will break the symmetry of HHG spectra (see blue lines in Fig. 4). However, this is quite different from the one observed in Ref. [52], where the left peak should be higher than the right peak; see the black lines in Fig. 4. Obviously, the asymmetry induced by the crystal axis offset does not explain all of the experimental observations. To reproduce the low temperature behavior, we note that there could be anisotropy in the CDW order parameters induced by disorder or strains. For the green lines shown in Fig. 4, we introduced a slight anisotropy in the CDW order parameters, i.e., $\Delta_{\mathbf{Q}_1} = 0.1148$ eV, $\Delta_{\mathbf{Q}_2} = 0.1147$ eV, and $\Delta_{\mathbf{Q}_3} = 0.1146$ eV, with the effective interaction strength $U_{\mathbf{Q}_1} = -1.80965$ eV, $U_{\mathbf{Q}_2} = -1.80935$ eV, and $U_{\mathbf{Q}_3} = -1.80905$ eV. The shape of the obtained HHG spectra reproduces the behavior observed in Ref. [52]. Particularly, the left peak now is higher than the right peak. We note that the center of mass shifts of H5 and H7 to the left and H3 to the right are also reproduced, although slightly overestimated. This suggests that the anisotropic CDW dominates over the offset effect in the low-temperature region, which could explain the

experimental observations.

Summary.—In conclusion, we have provided a theoretical explanation for the experimentally observed asymmetric behavior of HHG spectra for TiSe_2 in Ref. [52]. Specifically, we have proposed a simplified phenomenological mean-field model for this material, based on which the HHG spectra are calculated through the time-dependent Schrödinger equation. Our model is able to describe the double peak behavior of H5 and the single peak behavior in H3 and H7 as a function of laser polarization angle. For the low temperature phase, we find that the anisotropic CDW order reproduces the strongly asymmetric behavior of HHG spectra, which could be induced by the possible onset of strain at these temperatures that distorts the CDW phase. This work provides an important step towards establishing high harmonic spectroscopy as a powerful new tool to study the microscopic origins of correlations in materials such as the CDW orders.

The ICFO-QOT group acknowledges support from: ERC AdG NOQIA; MCIN/AEI (PGC2018-0910.13039/501100011033, CEX2019-000910-S/10.13039/501100011033, Plan National FIDEUA PID2019-106901GB-I00, Plan National STAMEENA PID2022-139099NB-I00 project funded by MCIN/AEI/10.13039/501100011033 and by the “European Union NextGenerationEU/PRTR” (PRTR-C17.I1), FPI); QUANTERA MAQS PCI2019-111828-2); QUANTERA DYNAMITE PCI2022-132919 (QuantERA II Programme co-funded by European Union’s Horizon 2020 program under Grant Agreement No. 101017733), Ministry of Economic Affairs and Digital Transformation of the Spanish Government through the QUANTUM ENIA project call – Quantum Spain project, and by the European Union through the Recovery, Transformation, and Resilience Plan – NextGenerationEU within the framework of the Digital Spain 2026 Agenda; Fundació Cellex; Fundació Mir-Puig; Generalitat de Catalunya (European Social Fund FEDER and CERCA program, AGAUR Grant No. 2021 SGR 01452, QuantumCAT \U16-011424, co-funded by ERDF Operational Program of Catalonia 2014-2020); Barcelona Supercomputing Center MareNostrum (FI-2023-1-0013); EU Quantum Flagship (PASQuanS2.1, 101113690); EU Horizon 2020 FET-OPEN OPTologic (Grant No. 899794); EU Horizon Europe Program (Grant Agreement 101080086 – NeQST), ICFO Internal “QuantumGaudi” project; European Union’s Horizon 2020 program under the Marie-Sklodowska-Curie grant agreement No. 847648; “La Caixa” Junior Leaders fellowships, “La Caixa” Foundation (ID 100010434); CF/BQ/PR23/11980043. Views and opinions expressed are, however, those of the author(s) only and do not necessarily reflect those of the European Union, European Commission, European Climate, Infrastructure and Environment Executive Agency

(CINEA), or any other granting authority. Neither the European Union nor any granting authority can be held responsible for them. U.B. acknowledges for the financial support of the IBM Quantum Researcher Program. R.W.C. acknowledges support from the Polish National Science Centre (NCN) under the Maestro Grant No. DEC-2019/34/A/ST2/00081. T.G. acknowledges financial support from the Agencia Estatal de Investigación (AEI) through Proyectos de Generación de Conocimiento PID2022-142308NA-I00 (EXQUSMI), and that this work has been produced with the support of a 2023 Leonardo Grant for Researchers in Physics, BBVA Foundation. The BBVA Foundation is not responsible for the opinions, comments, and contents included in the project and/or the results derived therefrom, which are the total and absolute responsibility of the authors. J.B. acknowledges financial support from the European Research Council for ERC Advanced Grant “TRANSFORMER” (788218), ERC Proof of Concept Grant “miniX” (840010), FET-OPEN “PETACom” (829153), FET-OPEN “OPTologic” (899794), FET-OPEN “TwistedNano” (101046424), Lasers4EU (101131771), MINECO for Plan Nacional PID2020-112664 GB-I00; QU-ATTO, 101168628; AGAUR for 2017 SGR 1639, MINECO for “Severo Ochoa” (CEX2019-000910-S), Fundació Cellex Barcelona, the CERCA Programme/Generalitat de Catalunya, and the Alexander von Humboldt Foundation for the Friedrich Wilhelm Bessel Prize. I.T. and J.B. acknowledge support from Marie Skłodowska-Curie ITN “smart-X” (860553).

END MATTERS

Tight-binding model of TiSe_2 .—For a full and comprehensive description of our approach, we provide a review of the tight-binding model. It has been introduced in Ref. [55], and gives the highest-lying valence band and the lowest-lying conduction band considered in our phenomenological mean-field model (1).

The crystal structure of the monolayer TiSe_2 is given by the primitive translation vectors $\mathbf{a}_1 = (\sqrt{3}a/2, -a/2)$ and $\mathbf{a}_2 = (0, a)$ with lattice constant $a = 3.54 \text{ \AA}$. In each unit cell, we have one Ti ion and two Se ions, Se(1) and Se(2). The corresponding positions are given by $\boldsymbol{\tau}_{\text{Ti}} = (0, 0, 0)$ and $\boldsymbol{\tau}_{\text{Se1}} = -\boldsymbol{\tau}_{\text{Se2}} = (a/2\sqrt{3}, -a/2, z_{\text{Se}})$ with $z_{\text{Se}} = 1.552 \text{ \AA}$, respectively.

The band structure of TiSe_2 is given by five bands based on the Ti $3d$ orbitals ($d_{x^2-y^2}, d_{3z^2-r^2}, d_{xy}, d_{yz}, d_{zx}$) above the Fermi level and six bands based on the $4p$ orbitals (p_x, p_y, p_z) of the Se(1) and Se(2) atoms below the Fermi level. In terms of these orbitals, the tight-

binding Hamiltonian is given by

$$H = \sum_{\mathbf{k}} \sum_{\mu\ell, \nu m} H_{\mu\ell, \nu m}(\mathbf{k}) c_{\mathbf{k}, \mu\ell}^\dagger c_{\mathbf{k}, \nu m}, \quad (7)$$

where $c_{\mathbf{k}, \mu\ell}^{(\dagger)}$ is the annihilation (creation) operator of an electron in orbital ℓ of atom μ at momentum \mathbf{k} . Here $H_{\mu\ell, \nu m}(\mathbf{k}) = \sum_{\mathbf{R}_n} E_{\mu\ell, \nu m}(\mathbf{R}_n) e^{-i\mathbf{k}\cdot\mathbf{R}_n}$ is the Fourier transform of the transfer integral $E_{\mu\ell, \nu m}(\mathbf{R}_n)$ in the Slater-Koster scheme [58] between the atomic orbitals $\mu\ell$ and νm at coordinate $\mathbf{R}_n = n_1\mathbf{a}_1 + n_2\mathbf{a}_2$ for integers n_1, n_2 . The energy levels of the atomic orbitals are given by $E_{\mu\ell, \mu\ell}(\mathbf{R}_n = 0) = \varepsilon_{\mu\ell}$.

Due to the octahedral structure of TiSe₂, we consider the energy levels $\varepsilon_{d\gamma}$, $\varepsilon_{d\varepsilon}$, and ε_p of the Ti $d\gamma$ ($d_{x^2-y^2}$, $d_{3z^2-r^2}$), Ti $d\varepsilon$ (d_{xy} , d_{yz} , d_{zx}), and Se p (p_x , p_y , p_z) orbitals, respectively. The transfer integrals $E_{\mu\ell, \nu m}(\mathbf{R}_n)$ are obtained through nine transfer integral parameters, $t(pd\sigma)$, $t(pd\pi)$, $t(dd\sigma)$, $t(dd\pi)$, $t(dd\delta)$, $t(pp\sigma)_1$, $t(pp\pi)_1$, $t(pp\sigma)_2$, and $t(pp\pi)_2$, where $t(pd\sigma)$ and $t(pd\pi)$ are the transfer integrals between the nearest-neighbor Ti $3d$ and Se $4p$ orbitals, and $t(dd\sigma)$, $t(dd\pi)$, and $t(dd\delta)$ are the transfer integrals between the nearest-neighbor Ti-Ti $3d$ orbitals. The subscripts 1 and 2 in $t(pp\sigma)$ and $t(pp\pi)$ indicate the transfer integrals between the nearest-neighbor Se(1)-Se(1) [Se(2)-Se(2)] $4p$ orbitals and between the nearest-neighbor Se(1)-Se(2) $4p$ orbitals, respectively. From Ref. [55], the optimized values of the transfer integral parameters for TiSe₂ are given by $\varepsilon_{d\varepsilon} = 0.2$ eV, $\varepsilon_{d\gamma} - \varepsilon_{d\varepsilon} = 1.112$ eV, $\varepsilon_{d\varepsilon} - \varepsilon_p = 2.171$ eV, $t(pd\sigma) = -1.422$ eV, $t(pd\pi) = 0.797$ eV, $t(dd\sigma) = -0.347$ eV, $t(dd\pi) = 0.119$ eV, $t(dd\delta) = -0.030$ eV, $t(pp\sigma)_1 = 0.709$ eV, $t(pp\pi)_1 = -0.103$ eV, $t(pp\sigma)_2 = 0.592$ eV, and $t(pp\pi)_2 = -0.009$ eV.

[1] P. B. Corkum, Phys. Rev. Lett. **71**, 1994 (1993).
[2] M. Lewenstein, P. Balcou, M. Y. Ivanov, A. L'Huillier, and P. B. Corkum, Phys. Rev. A **49**, 2117 (1994).
[3] F. Krausz and M. Ivanov, Rev. Mod. Phys. **81**, 163 (2009).
[4] T. Schultz and M. Vrakking, *Attosecond and XUV Physics: Ultrafast Dynamics and Spectroscopy* (Wiley, New York, 2014).
[5] S. Ghimire, A. D. DiChiara, E. Sistrunk, P. Agostini, L. F. DiMauro, and D. A. Reis, Nat. Phys. **7**, 138 (2011).
[6] O. Schubert, M. Hohenleutner, F. Langer, B. Urbaneck, C. Lange, U. Huttner, D. Golde, T. Meier, M. Kira, S. W. Koch, and R. Huber, Nat. Photonics **8**, 119 (2014).
[7] M. Hohenleutner, F. Langer, O. Schubert, M. Knorr, U. Huttner, S. W. Koch, M. Kira, and R. Huber, Nature **523**, 572 (2015).
[8] T. T. Luu, M. Garg, S. Y. Kruchinin, A. Moulet, M. T. Hassan, and E. Goulielmakis, Nature **521**, 498 (2015).
[9] G. Vampa, T. J. Hammond, N. Thiré, B. E. Schmidt, F. Légaré, C. R. McDonald, T. Brabec, and P. B. Corkum, Nature **522**, 462 (2015).

[10] G. Ndashimiye, S. Ghimire, M. Wu, D. A. Browne, K. J. Schafer, M. B. Gaarde, and D. A. Reis, Nature **534**, 520 (2016).
[11] H. Liu, Y. Li, Y. S. You, S. Ghimire, T. F. Heinz, and D. A. Reis, Nat. Phys. **13**, 262 (2016).
[12] Y. S. You, D. Reis, and S. Ghimire, Nat. Phys. **13**, 345 (2016).
[13] N. Yoshikawa, T. Tamaya, and K. Tanaka, Science **356**, 736 (2017).
[14] S. Ghimire and D. A. Reis, Nat. Phys. **15**, 10 (2018).
[15] F. Langer, M. Hohenleutner, C. P. Schmid, C. Poellmann, P. Nagler, T. Korn, C. Schüller, M. S. Sherwin, U. Huttner, J. T. Steiner, S. W. Koch, M. Kira, and R. Huber, Nature **533**, 225 (2016).
[16] J. Reimann, S. Schlauderer, C. P. Schmid, F. Langer, S. Baierl, K. A. Kokh, O. E. Tereshchenko, A. Kimura, C. Lange, J. Gädde, U. Höfer, and R. Huber, Nature **562**, 396 (2018).
[17] M. Baudisch, A. Marini, J. D. Cox, T. Zhu, F. Silva, S. Teichmann, M. Massicotte, F. Koppens, L. S. Levitov, F. J. García de Abajo, and J. Biegert, Nat. Commun. **9**, 1018 (2018).
[18] A. J. Uzan, G. Orenstein, Á. Jiménez-Galán, C. McDonald, R. E. F. Silva, B. D. Bruner, N. D. Klimkin, V. Blanchet, T. Arusi-Parpar, M. Krüger, A. N. Rubtsov, O. Smirnova, M. Ivanov, B. Yan, T. Brabec, and N. Dudovich, Nat. Photonics **14**, 183 (2020).
[19] G. Vampa, T. Hammond, N. Thiré, B. Schmidt, F. Légaré, C. McDonald, T. Brabec, D. Klug, and P. Corkum, Phys. Rev. Lett. **115**, 193603 (2015).
[20] A. A. Lanin, E. A. Stepanov, A. B. Fedotov, and A. M. Zheltikov, Optica **4**, 516 (2017).
[21] T. T. Luu and H. J. Wörner, Nat. Commun. **9**, 916 (2018).
[22] Y.-Y. Lv, J. Xu, S. Han, C. Zhang, Y. Han, J. Zhou, S.-H. Yao, X.-P. Liu, M.-H. Lu, H. Weng, Z. Xie, Y. B. Chen, J. Hu, Y.-F. Chen, and S. Zhu, Nat. Commun. **12**, 6437 (2021).
[23] F. Langer, M. Hohenleutner, U. Huttner, S. W. Koch, M. Kira, and R. Huber, Nat. Photonics **11**, 227 (2017).
[24] F. Langer, C. P. Schmid, S. Schlauderer, M. Gmitra, J. Fabian, P. Nagler, C. Schüller, T. Korn, P. G. Hawkins, J. T. Steiner, U. Huttner, S. W. Koch, M. Kira, and R. Huber, Nature **557**, 76 (2018).
[25] O. Neufeld, D. Podolsky, and O. Cohen, Nat. Commun. **10**, 405 (2019).
[26] T. Heinrich, M. Taucer, O. Kfir, P. B. Corkum, A. Staudte, C. Ropers, and M. Siviş, Nat. Commun. **12**, 3723 (2021).
[27] L. Yue, R. Hollinger, C. B. Uzundal, B. Nebgen, Z. Gan, E. Najafidehaghani, A. George, C. Spielmann, D. Kartashov, A. Turchanin, D. Y. Qiu, M. B. Gaarde, and M. Zuerch, Phys. Rev. Lett. **129**, 147401 (2022).
[28] G. Vampa, C. McDonald, G. Orlando, D. Klug, P. Corkum, and T. Brabec, Phys. Rev. Lett. **113**, 073901 (2014).
[29] U. Huttner, M. Kira, and S. W. Koch, Laser Photonics Rev. **11**, 1700049 (2017).
[30] S. Y. Kruchinin, F. Krausz, and V. S. Yakovlev, Rev. Mod. Phys. **90**, 021002 (2018).
[31] C. Yu, S. Jiang, and R. Lu, Adv. Phys. X **4**, 1562982 (2019).
[32] L. Yue and M. B. Gaarde, J. Opt. Soc. Am. B **39**, 535

- (2022).
- [33] R. E. F. Silva, I. V. Blinov, A. N. Rubtsov, O. Smirnova, and M. Ivanov, *Nat. Photonics* **12**, 266 (2018).
- [34] C. Orthodoxou, A. Zaïr, and G. H. Booth, *npj Quantum Materials* **6**, 76 (2021).
- [35] Y. Murakami, S. Takayoshi, A. Koga, and P. Werner, *Phys. Rev. B* **103**, 035110 (2021).
- [36] Y. Murakami, K. Uchida, A. Koga, K. Tanaka, and P. Werner, *Phys. Rev. Lett.* **129**, 157401 (2022).
- [37] K. Uchida, G. Mattoni, S. Yonezawa, F. Nakamura, Y. Maeno, and K. Tanaka, *Phys. Rev. Lett.* **128**, 127401 (2022).
- [38] M. Kanega, T. N. Ikeda, and M. Sato, *Phys. Rev. Res.* **3**, L032024 (2021).
- [39] J. Alcalá, U. Bhattacharya, J. Biegert, M. Ciappina, U. Elu, T. Graß, P. T. Grochowski, M. Lewenstein, A. Palau, T. P. H. Sidiropoulos, T. Steinle, and I. Tyulnev, *Proc. Natl. Acad. Sci.* **119**, e2207766119 (2022).
- [40] C. Shao, H. Lu, X. Zhang, C. Yu, T. Tohyama, and R. Lu, *Phys. Rev. Lett.* **128**, 047401 (2022).
- [41] F. J. Di Salvo, D. E. Moncton, and J. V. Waszczak, *Phys. Rev. B* **14**, 4321 (1976).
- [42] E. Morosan, H. W. Zandbergen, B. S. Dennis, J. W. G. Bos, Y. Onose, T. Klimczuk, A. P. Ramirez, N. P. Ong, and R. J. Cava, *Nat. Phys.* **2**, 544 (2006).
- [43] S. Y. Li, G. Wu, X. H. Chen, and L. Taillefer, *Phys. Rev. Lett.* **99**, 107001 (2007).
- [44] A. F. Kusmartseva, B. Sipos, H. Berger, L. Forró, and E. Tutiš, *Phys. Rev. Lett.* **103**, 236401 (2009).
- [45] Y. I. Joe, X. M. Chen, P. Ghaemi, K. D. Finkelstein, G. A. de la Peña, Y. Gan, J. C. T. Lee, S. Yuan, J. Geck, G. J. MacDougall, T. C. Chiang, S. L. Cooper, E. Fradkin, and P. Abbamonte, *Nat. Phys.* **10**, 421 (2014).
- [46] L. J. Li, E. C. T. O’Farrell, K. P. Loh, G. Eda, B. Özyilmaz, and A. H. Castro Neto, *Nature* **529**, 185 (2015).
- [47] H. Luo, W. Xie, J. Tao, I. Pletikovic, T. Valla, G. S. Sahasrabudhe, G. Osterhoudt, E. Sutton, K. S. Burch, E. M. Seibel, J. W. Krizan, Y. Zhu, and R. J. Cava, *Chem. Mater.* **28**, 1927 (2016).
- [48] T. E. Kidd, T. Miller, M. Y. Chou, and T.-C. Chiang, *Phys. Rev. Lett.* **88**, 226402 (2002).
- [49] K. Rossnagel, L. Kipp, and M. Skibowski, *Phys. Rev. B* **65**, 235101 (2002).
- [50] H. Cercellier, C. Monney, F. Clerc, C. Battaglia, L. Despont, M. G. Garnier, H. Beck, P. Aebi, L. Patthey, H. Berger, and L. Forró, *Phys. Rev. Lett.* **99**, 146403 (2007).
- [51] J. van Wezel, P. Nahai-Williamson, and S. S. Saxena, *Phys. Rev. B* **81**, 165109 (2010).
- [52] I. Tyulnev, L. Zhang, L. Vamos, J. Poborska, U. Bhattacharya, R. W. Chhajlany, T. Grass, S. Mañas-Valero, E. Coronado, M. Lewenstein, and J. Biegert, “High harmonic spectroscopy reveals anisotropy of the Mott to Charge-Density-Wave phase transition in TiSe₂,” arXiv:2409.04216.
- [53] D. Jérôme, T. M. Rice, and W. Kohn, *Phys. Rev.* **158**, 462 (1967).
- [54] C. Monney, H. Cercellier, F. Clerc, C. Battaglia, E. F. Schwier, C. Didiot, M. G. Garnier, H. Beck, P. Aebi, H. Berger, L. Forró, and L. Patthey, *Phys. Rev. B* **79**, 045116 (2009).
- [55] T. Kaneko, Y. Ohta, and S. Yunoki, *Phys. Rev. B* **97**, 155131 (2018).
- [56] C. Monney, C. Battaglia, H. Cercellier, P. Aebi, and H. Beck, *Phys. Rev. Lett.* **106**, 106404 (2011).
- [57] D. Moos, H. Jürß, and D. Bauer, *Phys. Rev. A* **102**, 053112 (2020).
- [58] J. C. Slater and G. F. Koster, *Phys. Rev.* **94**, 1498 (1954).